



## Hydrophobic dual metal silicate nanotubes for higher alcohol synthesis

Gaofeng Chen <sup>a</sup>, Olga A. Syzgantseva <sup>b,c</sup>, Maria A. Syzgantseva <sup>b,d</sup>, Li Peng <sup>e</sup>, Dragos Stoian <sup>f</sup>, Mo Li <sup>g,h</sup>, Isil Akpinar <sup>i</sup>, Guihua Yan <sup>a</sup>, Tianwei Xue <sup>e</sup>, Qishen Lyu <sup>a</sup>, Zhiwei Wang <sup>j</sup>, Tingzhou Lei <sup>k</sup>, Xianhai Zeng <sup>a,1,\*</sup>, Lu Lin <sup>a,1,\*</sup>, Shuliang Yang <sup>a,1,\*</sup>

<sup>a</sup> College of Energy, Xiamen University, Xiamen 361102, China

<sup>b</sup> Department of Chemistry, Lomonosov Moscow State University, Moscow 119991, Russia

<sup>c</sup> Peoples' Friendship University of Russia (RUDN University), 6 Miklukho-Maklaya st., Moscow 117198, Russia

<sup>d</sup> Department of Physics, Mendeleev University of Chemical Technology, Moscow 125047, Russia

<sup>e</sup> College of Chemistry and Chemical Engineering, Xiamen University, Xiamen 361005, China

<sup>f</sup> Swiss Norwegian Beamlines, European Synchrotron Radiation Facility, Grenoble 38000, France

<sup>g</sup> Telvent Control System (China) Co., Ltd, Beijing 100102, China

<sup>h</sup> Aveva China, Beijing 100102, China

<sup>i</sup> Department of Chemistry and International Institute of Nanotechnology, Northwestern University, 2145 Sheridan Road, Evanston, IL 60208, United States

<sup>j</sup> School of Environmental Engineering, Henan University of Technology, Zhengzhou 450001, China

<sup>k</sup> Institute of Urban and Rural Mining, Changzhou University, Changzhou 213164, China

<sup>1</sup> Fujian Engineering and Research Center of Clean and High-valued Technologies for Biomass, Xiamen Key Laboratory of Clean and High-valued Utilization for Biomass, Xiamen 361102, China

### ARTICLE INFO

### ABSTRACT

#### Keywords:

Hydrophobic modification  
Higher alcohol synthesis  
CO hydrogenation  
Bimetallic catalyst

Herein, a hydrophobic CuCoSNTs-c catalyst with hollow tubular structure and mesoporous wall was synthesized successfully for higher alcohol synthesis (HAS). The tubular CuCoSNTs-c was constructed with elaborately designed hydrophobic and aerophilic properties to suppress the formation of  $C_1$  molecules and enhance the CO conversion and  $C_{2+}OH$  selectivity. The mesoporous wall exposed the active sites sufficiently, and the macroscopic tubular channel improved the mass transfer kinetics and accelerated the desorption of alcohol products. Moreover, the hydrophobic and aerophilic tube wall could modulate the local microenvironment of CuCoSNTs-c, that is, enriching the  $H_2$  and CO molecules around the CuCo active sites and rapidly desorbing the in-situ produced water molecules in HAS. The hydrophobic multifunctional CuCoSNTs-c catalyst suppressed the selectivity of  $CO_2$  to less than 1.2%, while achieving a  $C_{2+}OH$  selectivity of up to 66.6% at a CO conversion of 80.4%. This catalyst demonstrated excellent stability for 360 h without obvious activity loss.

### 1. Introduction

Higher alcohols (HAs,  $C_{2+}OH$ ), which usually refer to alcohols containing two or more carbon atoms, are feedstocks for many high-value-added chemicals. HAs can be used as clean liquid fuels and gasoline additives, and have shown great application prospects [1]. Currently, they are mainly produced by sugar fermentation or hydration of petroleum-derived alkenes [2]. An alternative attractive way for HAs production is from syngas (CO and  $H_2$ ) conversion, which is a versatile, economical, and environmentally friendly route making full utilization of nonpetroleum carbon resources such as biomass, natural gas, shale gas and so on [3]. Recently, a new progress has been made in this

promising field. Several types of catalysts including but not limited to Mo-based catalysts [4,5], Rh-based catalysts [6,7], modified methanol synthesis catalysts and modified Fisher-Tropsch (F-T) synthesis catalysts (Co/Fe/Ni-based) [8–16] have been reported for higher alcohol synthesis (HAS) from syngas. Among them, the modified F-T CuCo-based catalysts have been proposed to be one of the most intriguing candidates for large-scale application owing to their high CO hydrogenation activity, abundant earth reserves, mild reaction conditions, low cost, and adjustable active sites [17–23]. For HAS, it is widely recognized that Co species are active centers for CO dissociation adsorption and carbon-carbon chain propagation to form  $C_xH_y^*$  intermediate, while Cu active sites are responsible for the formation of CO non-dissociative

\* Corresponding authors at: College of Energy, Xiamen University, Xiamen 361102, China.

E-mail addresses: [xianhai.zeng@xmu.edu.cn](mailto:xianhai.zeng@xmu.edu.cn) (X. Zeng), [lulin@xmu.edu.cn](mailto:lulin@xmu.edu.cn) (L. Lin), [ysl@xmu.edu.cn](mailto:ysl@xmu.edu.cn) (S. Yang).



adsorption activated species  $\text{CO}^*$ . The  $\text{CO}^*$  inserts into the  $\text{C}_x\text{H}_y^*$  to form critical  $\text{C}_x\text{H}_y\text{CO}^*$  intermediate, then further hydrogenates to produce HAs [17]. Due to the indispensable bifunctionality of CO insertion and CO dissociation for HAS, patterns of Cu-Co bimetallic catalysts with space proximity to fully utilize the different CO activation capabilities of Cu and Co sites have been proved to be a versatile and effective strategy to improve the catalytic performance.

Even though several effective strategies have been reported to prepare adjacent CuCo dual metal active sites from CuCo alloy species, such as perovskite-type oxides [24], co-precipitation oxides [25], layered double hydroxides [26–28],  $\text{CuCo}_2\text{O}_4$  spinel oxides [29] and metal-organic frameworks derived carbides [30,31]. CuCo alloy phase separation and nanoparticles aggregation often occur under relatively harsh reaction conditions due to the high surface energy of Cu as well as the low intermiscibility between Cu and Co. This will unavoidably result in catalyst deactivation with lower CO conversion and a decrease in HAs selectivity [19,32]. Besides, intricate reaction pathways including methanol synthesis, methanation, Fischer-Tropsch synthesis (FTS), and water-gas shift (WGS) reaction in syngas conversion significantly restrict the implementation and application of HAS from syngas [3]. Notably, during the HAS from syngas, the  $\text{CO}_2$  that is derived from the WGS reaction as the main by-product is often inevitable, which understandably deviated from the long-term pursuit of less carbon emission in the world.

In theory, promoting rapid desorption of water molecules from the catalyst surface will shift the sorption equilibrium of water [33], thereby effectively inhibit the  $\text{CO}_2$  formation. Rapid water desorption from the catalyst surface during syngas conversion will avoid the competitive adsorption between  $\text{H}_2\text{O}$  and CO reactants and release more active sites, which is a critical step in the HAS process. Furthermore, it has been demonstrated that the in-situ produced water molecules accelerated the sintering and agglomeration of Cu species, resulting in the instability of the catalyst [34,35]. Hence, the design of a hydrophobic catalyst to modulate reaction interface will be crucial for HAS from syngas. For catalysts, as fast mass transport and sufficiently exposed active sites at the gas-solid interface were critical for achieving excellent catalytic performance. Hierarchically hollow nanotube structure with open end and porous walls was therefore preferred for mass transfer because reactants could easily pass through these important channels and diffuse into the internal space to react on the active sites.

Based on the above insights, in this work, we developed a hierarchical hollow hydrophobic CuCo silicate nanotubes catalyst (denoted as CuCoSNTs-c hereafter) with mesoporous wall and mouth-open end by a

self-sacrificed template coupled with hydrophobic functionalization strategy. The CuCoSNTs-c with high hydrophobicity effectively restrained the WGS reaction, which further inhibited the formation of  $\text{CO}_2$  and enhanced the C-C coupling reaction. The chain growth probability was increased to 0.34, and the selectivity for undesired  $\text{C}_1$  by-product of  $\text{CO}_2$  was suppressed to 1.2%. Moreover, this hydrophobic CuCoSNTs-c catalyst displayed extraordinarily high catalytic activity for CO hydrogenation to HAs (CO conversion of 80.4%,  $\text{C}_2+\text{OH}$  selectivity of 66.6%,  $\text{C}_2+\text{OH}$  space-time yield (STY) of 0.970 g/g<sub>cat</sub>·h), as well as longstanding stability within 360 h on-stream, which is greatly superior to most of the recently reported catalysts for HAS (Table S6).

## 2. Experimental methods

### 2.1. Preparation of hierarchical CuCo silicate CuCoSNTs

The CuCoSNTs was prepared in one-pot procedure through a solvothermal method with some modifications [36–38]. 0.1 mmol copper (II) chloride dihydrate, 0.1 mmol cobalt (II) chloride hexahydrate, ammonia chloride (5 mmol), and  $\text{NH}_3\cdot\text{H}_2\text{O}$  (0.5 mL) were mixed in 30 mL of deionized water to form a clear solution. Meanwhile, 0.05 g SNTs was ultrasonicated homogeneously and dispersed in 20 mL of deionized water. These two solutions were mixed and transferred into a Teflon-lined autoclave at 140 °C for 6 h. The solid product was collected by centrifugation and rinsed with distilled water three times. Finally, the product was dried in a vacuum oven at 60 °C overnight for further use.

### 2.2. Preparation of hydrophobic CuCoSNTs-c

Hydrophobic functionalization was achieved by an organic component modification. In a typical process, 0.05 g CuCoSNTs was activated in a vacuum oven at 150 °C for 11 h. After cooling to 30 °C, 2 mL n-hexane and 0.1 g diethoxydimethylsilane (DEMS) were mixed with the activated CuCoSNTs, and the mixture was sonicated (40 kHz, 400 W) at room temperature for 3 h. The obtained product was washed with n-hexane three times and dried in a vacuum oven at 80 °C for 12 h. The obtained catalyst was named as CuCoSNTs-c without any further calcination and reduction treatment. All catalysts employed and characterized in this work were freshly obtained catalysts.

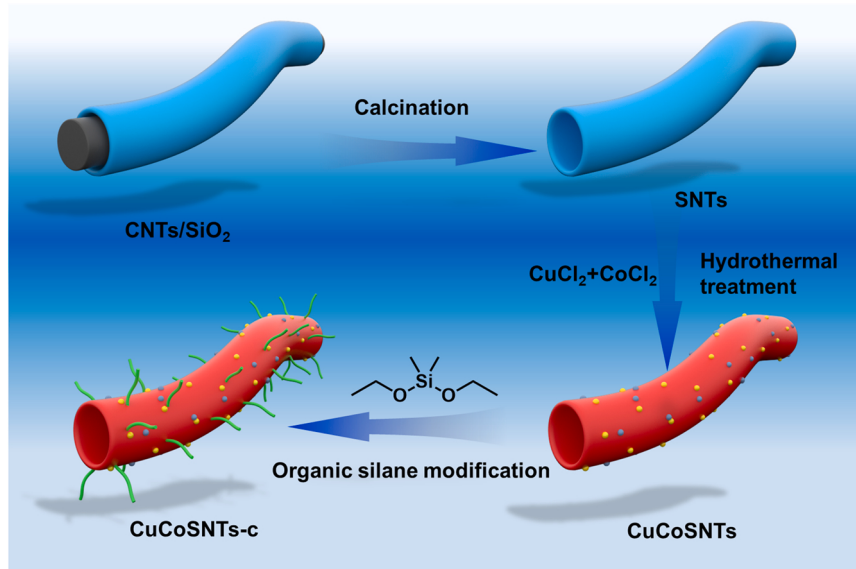
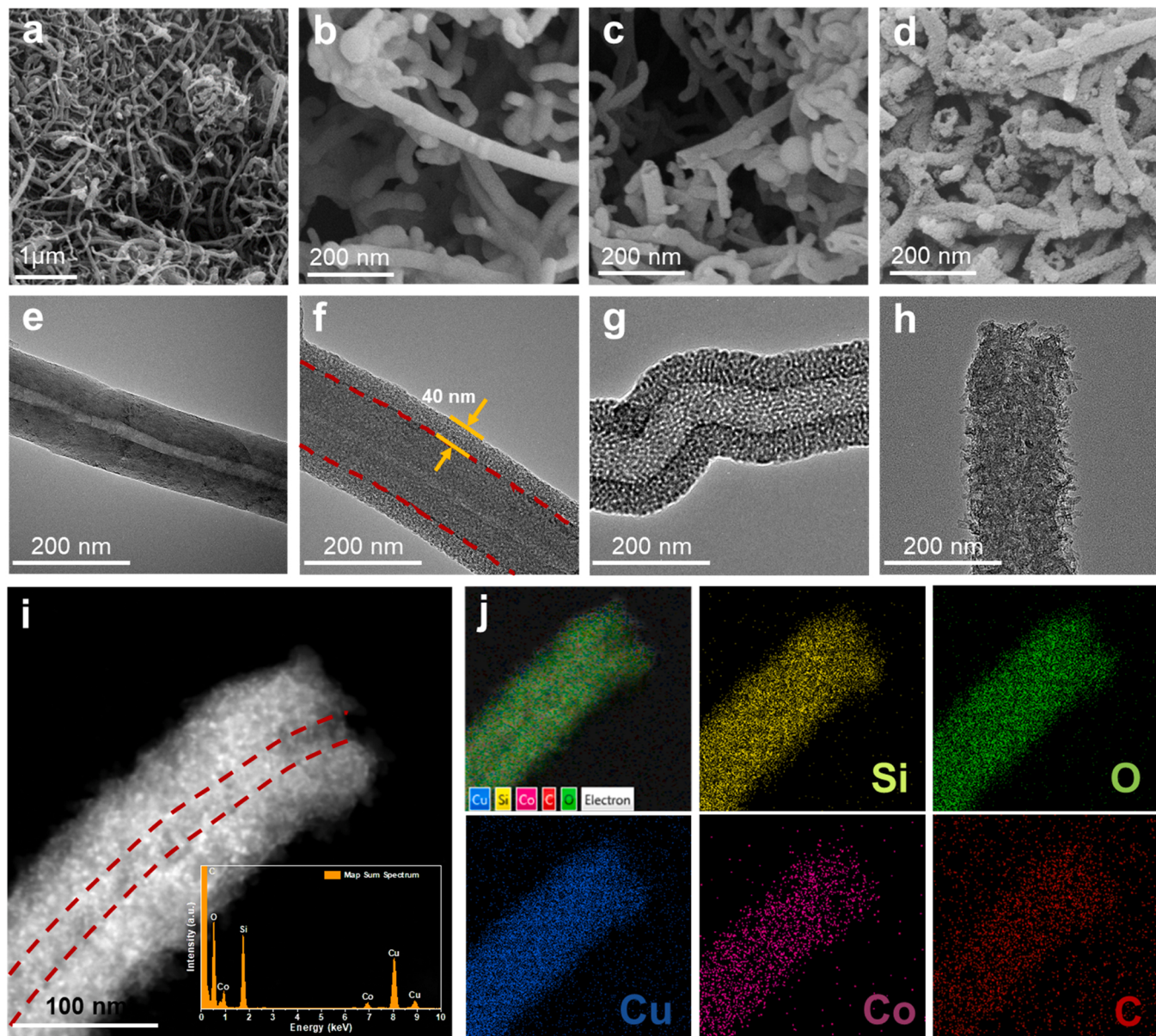


Fig. 1. Schematic illustration of the synthesis of hydrophobic catalyst CuCoSNTs-c.



**Fig. 2.** Morphology and structure characterizations. SEM images of CNTs (a), CNTs/SiO<sub>2</sub> (b), SNTs (c), and CuCoSNTs-c (d). TEM images of CNTs (e), CNTs/SiO<sub>2</sub> (f), SNTs (g), and CuCoSNTs-c (h). HAADF-STEM image (i) of CuCoSNTs-c and the corresponding EDS elemental mappings (j).

### 2.3. Computational details

The reaction mechanism was studied within the density functional theory (DFT) applying Perdew-Burke-Ernzerhof (PBE) [39] density functional, as implemented in Quantum Espresso (QE) code [40]. To represent the wavefunctions and charge density plane wave basis set with the cutoffs of 40 Ry and 320 Ry was employed. 2x2x2 and 2x2x1 Monkhorst-Pack k-point grids were used to sample the reciprocal space for the bulk and surface models of SiO<sub>2</sub>, respectively, while 4x4x1 grid was employed for the electronic structure calculations. The interaction between the valence electrons and core region was described using the ultrasoft pseudopotentials [41, 42]. The initial structure of  $\alpha$ -quartz SiO<sub>2</sub> was taken from the previous work [43] and fully optimized both in terms of the cell parameters and atomic positions with the given computational protocol. To represent a fragment of silica nanotube, the (001) surface slab of SiO<sub>2</sub> was cut out, this being an adequate model of the nanotube due to their large diameter of about 100 nm. To maintain the charge neutrality, both sides of the slab were hydroxylated by adding

protons to the superficial oxygen atoms. To construct the model of the CuCo catalyst site that were exposed to the reactants, the Cu and Co atoms were deposited on the SiO<sub>2</sub> surface on top of terminal oxygen atoms in place of hydroxyl groups in order to maintain the 2+ formal charge of both metal ions. The vacuum thickness of at least 12 Å was used in all calculations. The atomic position of all surface models with and without adsorbates are fully relaxed. The structural models are presented in Fig. S24.

The reported energies of formation of adsorbed reaction intermediates were computed as follows with respect to the pristine catalyst surface and gas phase CO, H<sub>2</sub>, H<sub>2</sub>O:

$$\Delta_E = E_{\text{surf+ads}} - E_{\text{surf}} - nE_{\text{CO}_2} - mE_{\text{H}_2} + pE_{\text{H}_2\text{O}}$$

To model the effect of the hydrophobic coating achieved by the silanization (see Fig. S11) of the SiO<sub>2</sub> surface, a Born-Oppenheimer molecular dynamics simulation of the coated surface containing Si-(CH<sub>3</sub>)<sub>2</sub> fragments in the presence of water molecules was performed for about 13 ps at the temperature of 70 °C, employing xTB approach [44]

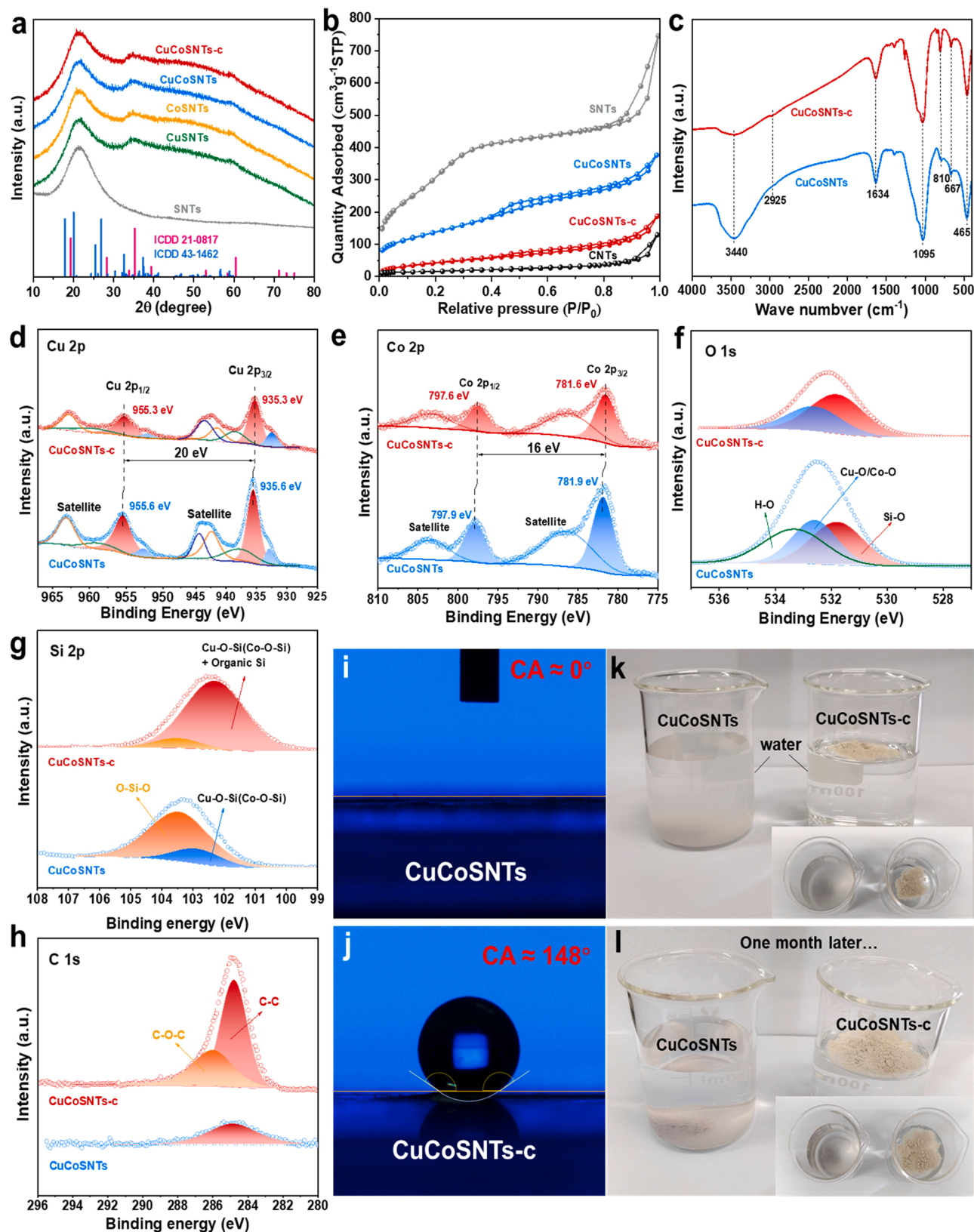


**Fig. 3.** (a) XRD patterns of diverse catalysts and SNTs. (b) N<sub>2</sub> adsorption-desorption isotherm of CNTs, SNTs, CuCoSNTs and CuCoSNTs-c. (c) FTIR spectra of the CuCoSNTs and CuCoSNTs-c. High-resolution XPS spectra of CuCoSNTs and CuCoSNTs-c for (d) Cu 2p, (e) Co 2p, (f) O 1s, (g) Si 2p, and (h) C 1s. (i, j) Water-droplet contact angle test of CuCoSNTs and CuCoSNTs-c. (k, l) Photographs of CuCoSNTs-c and CuCoSNTs dispersed in deionized water, initially and one month later.

along with Grimme's [45] dispersion correction, as implemented in CP2K code [46]. All structures are visualized with the VESTA [47] or VMD [48] codes.

### 3. Results and discussion

#### 3.1. Synthesis and structural characterization of CuCoSNTs-c

The synthetic procedure for hydrophobic Cu-Co bimetallic silicate nanotube is illustrated in Fig. 1. Overall, the preparation route contains three steps. Firstly, hierarchical hollow mesoporous  $\text{SiO}_2$  nanotubes (SNTs) (Fig. S1) were prepared with carbon nanotubes (CNTs) (Fig. S2) as the self-sacrificed template after calcining at 600 °C for 5 h in air (Fig. S3), with the assistance of tetraethyl orthosilicate (TEOS) as the silica source and cetyl trimethyl ammonium bromide (CTAB) as the porogen under the weak alkaline environment [36,49]. The CNTs/ $\text{SiO}_2$  inherited the tubular morphology structure of CNTs, as shown in Fig. S4. The inner diameter of SNTs is correlated to the outer diameter of CNTs as the silica layer was grown on the CNTs outer wall, as shown in Figs. S1–2. In the second step, dual metal CuCoSNTs with mouth-open end and tubular morphology was constructed by a mild hydrothermal reaction. In this step,  $\text{Cu}^{2+}$  ions and  $\text{Co}^{2+}$  ions in the solution easily diffused into the pores of the SNTs and reacted with  $\text{SiO}_2$  to form copper silicate and cobalt silicate in-situ [36]. After a hydrophobic functionalization modification of the CuCoSNTs with diethoxydimethylsilane (DEMS), the hydrophobic CuCoSNTs-c catalyst was successfully obtained. It should be noted that this design of the hollow mouth-open end of CuCoSNTs-c will be significantly conducive to the barrier-free shuttle of the reactive syngas molecules, and the hydrophobic modification will facilitate the diffusion and desorption of the produced higher alcohols.

The morphology evolutions of the prepared materials in each step are displayed in Fig. 2. Fig. 2a showed a representative SEM image of the wormlike CNTs template with smooth surface and diameter between 60 nm and 100 nm (Fig. 2e). The SEM image of the mesoporous silica shell encapsulated CNTs is shown in Fig. 2b. The TEM image revealed that the CNTs were evenly coated with a layer of mesoporous  $\text{SiO}_2$  shell about 40 nm thickness (Fig. 2f). After removing CTAB and CNTs templates, the prepared mesoporous silica nanotubes (SNTs) exhibited a morphology with a hollow mouth-open end and hierarchical pore structure (Fig. 2c). The high-resolution TEM (HRTEM) image showed large number of wormlike mesopores are present in the 40 nm-thickness walls with a wide hollow channel in the center of SNTs (Fig. 2g). Through a hydrothermal treatment, the CuCoSNTs metal silicate (Fig. S5) was in-situ formed by virtue of the diffusion of metal ions into the pore of the SNTs and reacted with silica species. Followed by a further organic hydrophobically functionalized modification with DEMS, hydrophobic CuCoSNTs-c was obtained. The hydrophobic modification had negligible influence on the morphology and pore structure of CuCoSNTs (Figs. S5, 2d, h). The SEM image revealed that the surface of the CuCo silicate catalyst became rough (Fig. 2d). The TEM image of CuCoSNTs-c showed its hollow mouth-open end structure with thin nano petals connecting along the wall of the SNTs materials (Fig. 2h). High-angle annular dark-field scanning TEM (HAADF-STEM) images exhibited the hollow nanotube-like structure with mouth-open end morphology (Fig. 2i), and the corresponding energy-dispersive X-ray spectroscopy (EDS) mapping confirmed the uniform dispersion of Cu, Co, and C throughout the mesoporous SNTs matrix in CuCoSNTs-c (Fig. 2j). The Cu and Co metal contents in hydrophilic catalyst CuCoSNTs were 12.1 and 11.8 wt% correspondingly, determined by inductively coupled plasma mass spectrometry (ICP-MS) (Table S1). As shown in Table S1, the Cu and Co contents were determined to be 11.6 and 11.7 wt% after adding hydrophobic counterparts in the CuCoSNTs-c catalyst, respectively. These results indicate that the mild hydrophobic modification will not affect the metal content. For comparison, single metal CuSNTs-c and CoSNTs-c were also synthesized following a similar method, but with only copper (II) chloride dihydrate or cobalt (II) chloride hexahydrate as

the metal silica precursor. Both the CuSNTs-c and CoSNTs-c demonstrated the hollow mouth-open end structure and uniform dispersion of Cu, Si, O, C, and Co, Si, O, C, which were similar to the CuCoSNTs-c (Figs. S6 and S7).

X-ray diffraction (XRD) pattern of materials including CNTs, CNTs/ $\text{SiO}_2$ , SNTs, CuSNTs, CoSNTs, CuCoSNTs, and CuCoSNTs-c are displayed in Fig. 3a and S8. The CNTs had a typical diffraction peak at 26°, whereas CNTs/ $\text{SiO}_2$  showed a broad peak at 23° owing to the introduction of amorphous silica coating layer. After burning off the CNTs, the obtained SNTs exhibited a broad peak of the amorphous  $\text{SiO}_2$  and a peak at 26° was not observed, indicating the complete removal of CNTs. The CuCoSNTs displayed low crystallinity with weak and broad reflections of the highly dispersed cobalt silicate (ICDD 21–0871) and copper silicate (ICDD 43–1462) at 20 of ~33° and 60°, corresponding to the amorphous characteristics of metal silicate [50–54] (Fig. 3a). This amorphous structure was also confirmed by SEM and TEM (Fig. 2). The CuCoSNTs-c showed similar diffraction characters as CuCoSNTs, which indicated the hydrophobic modification had negligible impact on the morphology structure and phase composition. The reduction temperature of copper silicate is at 312 °C, while that of cobalt silicate is higher at 838 °C. The  $\text{H}_2$ -TPR characterization further confirmed that the catalysts we prepared were copper silicate and cobalt silicate [17] (Fig. S9). The porosities of the CNTs, SNTs, CuCoSNTs, and CuCoSNTs-c were further characterized via the  $\text{N}_2$  adsorption-desorption isotherms (Fig. 3b). CNTs showed the lowest surface area ( $56 \text{ m}^2/\text{g}$ ) without obvious mesoporous characters. However, the SNTs had the highest surface area of  $1127 \text{ m}^2/\text{g}$ , which is due to the abundant mesoporous channels. The CuCoSNTs and CuCoSNTs-c display typical IV isotherms with type H<sub>3</sub> hysteresis loops since the  $\text{Cu}^{2+}$  ions and  $\text{Co}^{2+}$  ions in the reaction solution easily diffused into the pore of the SNTs and reacted with  $\text{SiO}_2$  to form copper silicate and cobalt silicate in-situ. The hydrophobic CuCoSNTs-c exhibited a surface area of  $162 \text{ m}^2/\text{g}$ , which is lower than the unmodified CuCoSNTs with surface area of  $499 \text{ m}^2/\text{g}$ . This reduced surface area strongly implied that the successful modification of organic silane on the CuCoSNTs. More detailed information about porosities of other control samples and the corresponding pore size distribution are provided in Fig. S10 and Table S2.

After hydrophobic modification, changes of the surface properties in both CuCoSNTs and CuCoSNTs-c were further characterized by Fourier transform infrared (FTIR) spectra (Fig. 3c). The absorption bands at 465 and  $667 \text{ cm}^{-1}$  were assigned to the vibration of Cu-O or Co-O bands in the copper silicate or cobalt silicate, and the bands at 810 and  $1095 \text{ cm}^{-1}$  attributed to the vibration of Si-O-Si bands in the mesoporous SNTs. Moreover, the strong -OH stretch at  $3440 \text{ cm}^{-1}$  related to the isolated silanol group on CuCoSNTs provided plentiful active sites to introduce hydrophobic -CH<sub>3</sub> groups through a facile silanization reaction (Fig. S11). FTIR demonstrated that the new appeared absorption band at  $2925 \text{ cm}^{-1}$  for hydrophobic CuCoSNTs-c when compared to the unmodified CuCoSNTs, which was attributed to the vibration of introduced -CH<sub>3</sub> groups [9,55]. These results explicitly indicated that the successful modification of hydrophobic organic silicate groups on the CuCoSNTs-c sample was achieved.

X-ray photoelectron spectroscopy (XPS) was further carried out to characterize the elemental composition and surface chemical state. The high-resolution XPS scan of Cu 2p<sub>3/2</sub> exhibited a dominant peak at 935.6 eV accompanied by characteristic satellite peaks (937.9 eV, 942.4 eV, and 944.4 eV), which signified a Cu species in Cu-O-Si network of copper silicate [54,56–59]. While a peak at 933.1 eV was attributed to CuO<sub>x</sub> ( $x \approx 2$ ) [54,56,59–61], which can be attributed to a shift in the binding energy (BE) position caused by a modification in the coordination environment (Fig. 3d and S12a). However, the BE of Cu 2p<sub>3/2</sub> in the CuCoSNTs slightly shifted toward a higher BE compared with that of CuCoSNTs-c. Amorphous cobalt silicate had a structure similar to that of Co(OH)<sub>2</sub>, and the coordination environment of Co in silicate was certainly similar to that of Co(OH)<sub>2</sub>, with O-Co-O bonds. Therefore, a peak-fitting principle similar to that of Co(OH)<sub>2</sub> can be adopted. The Co

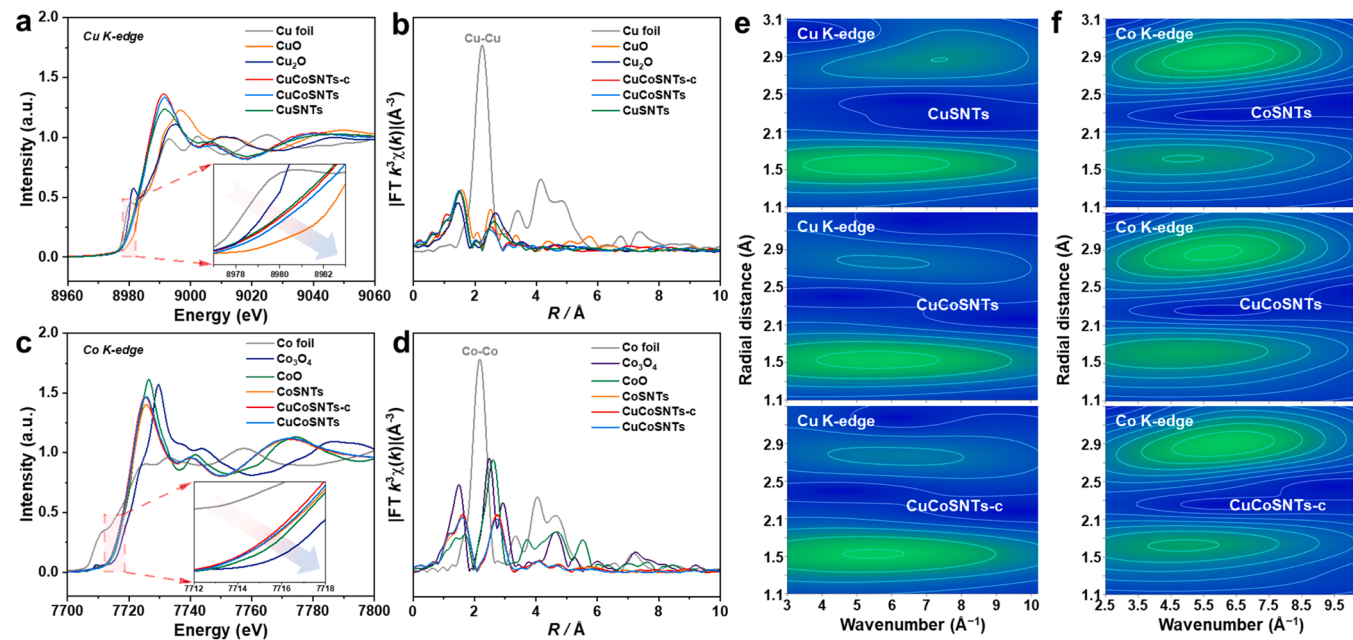


**Fig. 4.** Detailed electronic structure analysis of CuSNTs, CoSNTs, CuCoSNTs, and CuCoSNTs-c. (a) Cu K-edge XANES spectra of CuSNTs, CuCoSNTs, CuCoSNTs-c, Cu foil, Cu<sub>2</sub>O, and CuO. (b) Fourier-transformed (FT)  $k^3$ -weighted EXAFS (uncorrected for phase-shift) spectra for Cu K-edge of CuSNTs, CuCoSNTs, CuCoSNTs-c, Cu foil, Cu<sub>2</sub>O, and CuO. (c) Co K-edge XANES spectra of CoSNTs, CuCoSNTs, CuCoSNTs-c, Co foil, CoO, and Co<sub>3</sub>O<sub>4</sub>. (d) FT  $k^3$ -weighted EXAFS (uncorrected for phase-shift) spectra for Co K-edge of CoSNTs, CuCoSNTs, CuCoSNTs-c, Co foil, CoO, and Co<sub>3</sub>O<sub>4</sub>. (e) Wavelet-transformed  $k^3$ -weighted EXAFS spectra for Cu K-edge of CuSNTs, CuCoSNTs, and CuCoSNTs-c. (f) Wavelet-transformed  $k^3$ -weighted EXAFS spectra for Co K-edge of CoSNTs, CuCoSNTs, and CuCoSNTs-c.

2p<sub>3/2</sub> and Co 2p<sub>1/2</sub> peaks of CuCoSNTs-c were observed at 781.6 eV and 797.6 eV, respectively, with a spin-orbital splitting separation of 16.0 eV ( $\Delta E_{Co}$ ) (Table S3). In addition to the main peaks, there are also satellite peaks associated with plasmon losses and final state effects. These results suggested that Co mainly presented in the Co(OH)<sub>2</sub> state [62–65], which was consistent with the presence of cobalt silicate (Fig. 3e and S12b) [66–68]. Similarly, the BE of Co 2p<sub>3/2</sub> in the CuCoSNTs-c shifted toward a bit lower (~0.3 eV) valence state than that of CuCoSNTs (Fig. 3e). As shown in Fig. S12, the hydrophobic modification also slightly reduced the valence state of the Cu and Co in the CuSNTs and CoSNTs. The BEs of Cu 2p<sub>3/2</sub> in CuSNTs and CuCoSNTs were found to be similar. The BEs of Co 2p<sub>3/2</sub> of CoSNTs and CuCoSNTs were consistent. These results indicate that the hydrophobic organic silane modification could modulate the electronic valence state of the active sites. However, this electronic regulation effect was very weak, indicated by the BEs shift of only 0.3 eV. As shown in the X-ray excited Auger spectra (Fig. S13), the value of Cu LMM of catalysts was at ~915 eV, which provided further confirmation of the successful preparation of copper silicate [17,69]. The peaks observed at 531.8 eV, 532.6 eV, and 533.3 eV can be attributed to Si-O, Cu-O/Co-O, and O-H, respectively, as reported in previous studies (Fig. 3f) [65,70,71]. These results confirmed the presence of cobalt silicate and copper silicate in CuCoSNTs, providing further evidence of the successful synthesis of CuCoSNTs. Additionally, the hydrophobic modification of metal silicate led to the disappearance of surface O-H, indicating the successful modification of -CH<sub>3</sub> onto the catalyst. The formation of copper silicate and cobalt silicate were also demonstrated by Si 2p XPS spectra (Figs. 3g and S14a). The presence of the peak at 102.3 eV for CuCoSNTs was assigned to the copper silicate and cobalt silicate. The prominent peak shift from 103.5 eV (O-Si-O) for CuCoSNTs to 102.3 eV (Cu/Co-O-Si or organic Si) for CuCoSNTs-c was attributed to the successful modification of hydrophobic organic silicate [38]. As shown in Fig. S14b, the sp<sup>2</sup> bonding was obvious for CNTs owing to the conjugated benzene ring structure [72]. The C 1s spectrum of the CuCoSNTs-c was deconvoluted into C-C (284.8 eV) and C-O-C (286.0 eV) (Fig. 3h), suggesting the successful grafting of organic silicate. These results were also confirmed

from the atomic percentages from XPS in Table S4.

The water-droplet contact angle (CA) test was also conducted to characterize the hydrophobicity of CuCoSNTs and CuCoSNTs-c. The CuCoSNTs exhibited a contact angle of 0° (Fig. 3i), implying a superhydrophilic surface with the siphon phenomenon of porous materials. After the hydrophobic modification, the CA sharply increased to about 148° over the CuCoSNTs-c surface (Fig. 3j), indicating that the superhydrophilic surface of CuCoSNTs had been completely converted to the hydrophobic surface of CuCoSNTs-c after DEMS modification. Although hydrophilic CuCoSNTs were well dispersed in deionized water (DW), it was problematic for DW to infiltrate the hydrophobic surface of CuCoSNTs-c, and it formed a long-lasting separate phase (Fig. 3k, l). For comparison, single metal CuSNTs and CoSNTs were also modified with DEMS. Although the surfaces of CuSNTs and CoSNTs were superhydrophilic with CAs about zero degree, the CAs of both CuSNTs-c and CoSNTs-c surface increased obviously to 132° and 138°, respectively (Fig. S15). These positive results evidently demonstrated that this DEMS modification method was also compatible with the hydrophobic modification of single metal silicates.

Synchrotron-radiation-based X-ray adsorption fine structure (XAES) included X-ray adsorption near-edge structure spectroscopy (XANES) and extended X-ray fine structure spectroscopy (EXAFS) were performed to further interpret the detailed electronic structure and coordination environment of Cu and Co in different catalysts. As shown in Fig. 4a, the near-edge adsorption thresholds of Cu K-edge in CuSNTs, CuCoSNTs, and CuCoSNTs-c were located between Cu<sub>2</sub>O and CuO, suggesting that the valence states of Cu sites in these catalysts were between Cu<sup>1+</sup> and Cu<sup>2+</sup>. The position of the rising edge of CuCoSNTs is slightly positive shifted in comparison with CuSNTs (inset of Fig. 4a), revealing that the Cu atoms in CuCoSNTs modified by Co had more positive charge compared with CuSNTs due to exceptionally weak electronic transfer from Cu to Co. Moreover, the position of the rising edge of CuCoSNTs-c is negatively shifted compared to CuCoSNTs (inset of Fig. 4a), implying a slightly rich electronic state after hydrophobic modification. As shown in the Fourier transform (FT)  $k^3$ -weighted EXAFS spectra, the prominent peaks of CuSNTs, CuCoSNTs, and CuCoSNTs-c were located at about

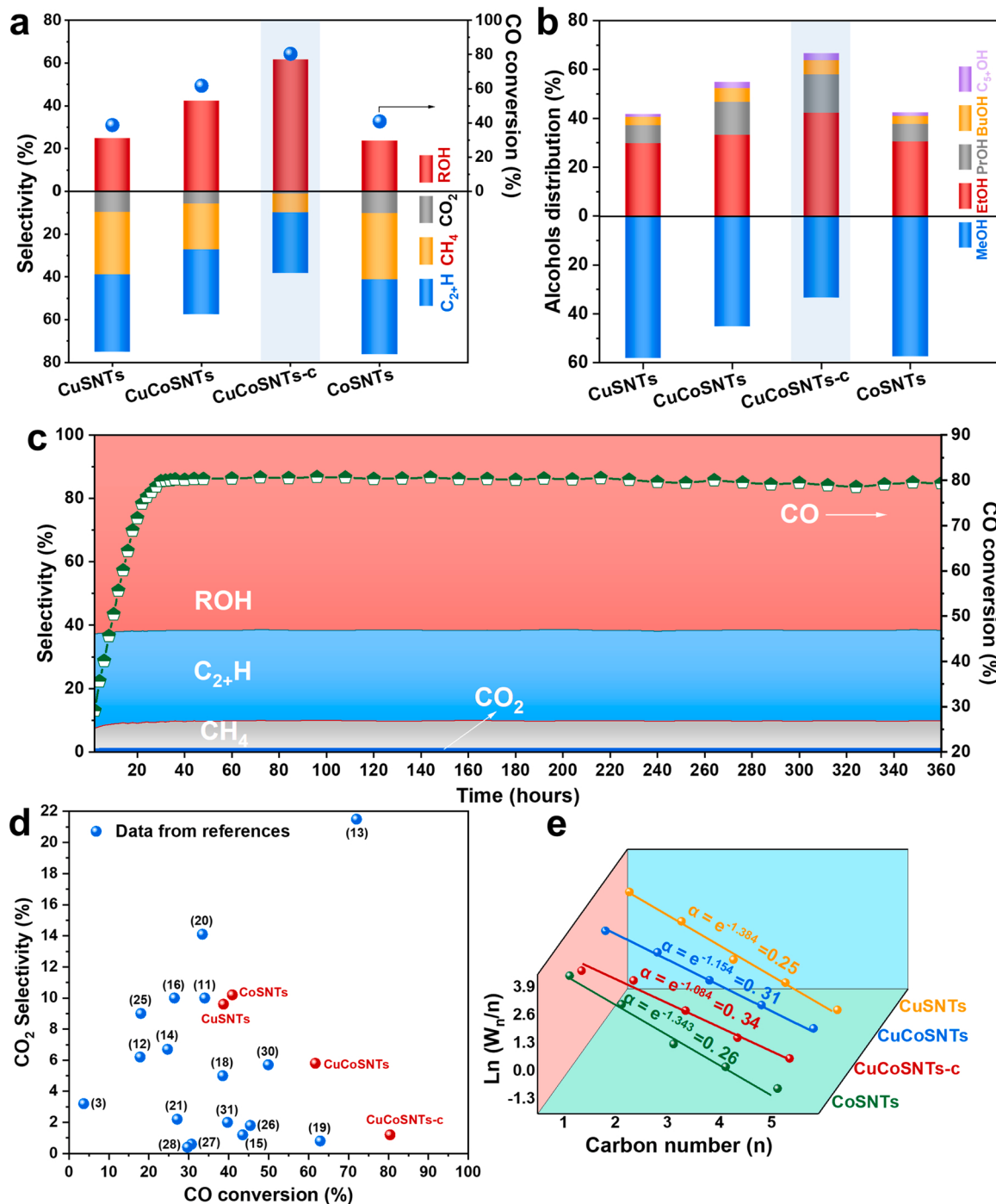


**Fig. 5.** Catalytic results in higher alcohol production from syngas. (a) Catalytic activity and product selectivity (including  $\text{CO}_2$ ). (b) Detailed selectivity distribution of alcohols product. (c) Stability test of the hydrophobic CuCoSNTs-c catalyst. (d) CO conversion,  $\text{CO}_2$  selectivity and (e) ASF plots over different catalysts. Reaction conditions: 270 °C, 3 MPa, 8000 h<sup>-1</sup>,  $\text{H}_2/\text{CO} = 2/1$ .

1.51 Å, 1.49 Å, and 1.50 Å, which stemmed from the scattering of Cu-O path, without the appearance of the Cu-Cu scattering at 2.24 Å, indicating a very weak micro-environment modification from Co and C (Fig. 4b). The second peaks were located at about 2.50 Å derived from the scattering of Cu-O-Si for CuSNTs, CuCoSNTs, and CuCoSNTs-c. However, this electronic regulation effect was negligible due to the proximity of the adsorption thresholds of Cu K-edge in these catalysts (inset of Fig. 4a). This result matched well with the above XPS analysis. The wavelet transformed plots (WT, Fig. 4e, S16) were conducted to further analyze the Cu K-edge EXAFS oscillation. WT is often used to ascertain the contribution of a certain pathway in both R-space and k-

space at the same time [22]. The intensity at about 5.5 Å<sup>-1</sup> and 6.0 Å<sup>-1</sup> (around 7.0 Å<sup>-1</sup> for CuSNTs) were ascribed to the Cu-O bond and Cu-O-Si bond in the Cu WT contour plot of CuSNTs, CuCoSNTs, and CuCoSNTs-c, and the Cu-Cu signal at about 7.2 Å<sup>-1</sup> was not observed, implying the absence of Cu-Cu bond.

XAES measurement was further performed to investigate the electronic state of Co over catalysts CoSNTs, CuCoSNTs, and CuCoSNTs-c. Several standard Co species (e.g., Co foil, CoO, and  $\text{Co}_3\text{O}_4$ ) were employed as references. The rising edge adsorption thresholds of Co K-edge in CoSNTs, CuCoSNTs, and CuCoSNTs-c were situated near CoO, revealing the Co oxidation state in all three catalysts is in fact very close

to the +2 valence state (Fig. 4c). However, the position of the rising edge for the CuCoSNTs was slightly negative than that in CoSNTs (inset of Fig. 4c), implying that the Co species in CuCoSNTs modified by Cu had more electrons due to electronic very weakly withdrawal from Cu. Moreover, the edge position of CuCoSNTs-c is slightly negative shifted compared to CuCoSNTs (inset of Fig. 4c), implying a slightly rich electronic state after hydrophobic modification, which was in accordance with the XPS result. However, this electronic regulation effect was insignificant owing to the adjacent of the pre-edge adsorption thresholds of Co K-edge in these catalysts (inset of Fig. 4c). As shown in FT k<sup>3</sup>-weighted EXAFS spectra, one main peak at about 1.63 Å attributed to Co-O shell scattering could be observed in CoSNTs, CuCoSNTs, and CuCoSNTs-c, without the appearance of the Co-Co scattering (2.18 Å), indicating that there was no formation of metal Co (Fig. 4d). The second peak was located at about 2.71 Å that was derived from the scattering of Co-O-Si for CoSNTs, CuCoSNTs, and CuCoSNTs-c. Furthermore, the WT was conducted to analyze the Co K-edge EXAFS oscillation (Fig. 4f, S17). The intensity at ca. 4.8 Å<sup>-1</sup> and 5.7 Å<sup>-1</sup> were assigned to the Co-O bond and Co-O-Si bond in the Co WT contour plot of CoSNTs, CuCoSNTs, and CuCoSNTs-c, and the Co-Co signal at about 7.3 Å<sup>-1</sup> was not observed, inferring the absence of Co-Co bond. Overall, compared with single metal Cu or Co catalyst, bimetallic CuCo catalyst and hydrophobic functionalization modified had a slight effect on the morphology, structure, and electronic properties of the catalyst.

### 3.2. The catalytic performance in HAS

The catalytic performance of different freshly prepared catalysts for HAS from syngas was tested on a Micro-activity Effi with a tubular fixed-bed reactor (Fig. S18). Reaction conditions including reaction temperature, total pressure, and gas hourly space velocity (GHSV) were taken into consideration to achieve the optimal catalytic performance (Fig. S19). For the hydrophobic CuCoSNTs-c catalyst, the CO conversion increased with the enhanced reaction temperature. However, the selectivity of alcohols decreased continuously, along with an increased selectivity of CH<sub>4</sub> and CO<sub>2</sub> (Fig. S19a). At 270 °C, the yield of alcohols reached as high as 49.6% at a CO conversion of 80.4%. Although it was beneficial for the higher alcohol synthesis with increasing reaction pressure (Fig. S19b), it generally required more sophisticated reaction equipment to implement the high-pressure reaction accompany with higher energy consumption. The CO conversion was decreased with increasing GHSV (Fig. S19c), owing to the shorter residence reaction time. The selectivity of alcohols was increased and then decreased with increasing GHSV, accompanied by a decreased CH<sub>4</sub> and CO<sub>2</sub>. In summary, as for the hydrophobic catalyst CuCoSNTs-c, the best reaction conditions were determined to be a reaction temperature of 270 °C, a total pressure of 3 MPa, and a GHSV of 8000 h<sup>-1</sup>.

The catalytic performances of hydrophilic catalysts (CuSNTs, CoSNTs, and CuCoSNTs) and hydrophobic catalyst CuCoSNTs-c were also systematically evaluated under the optimum reaction conditions of 270 °C, 3 MPa, 8000 h<sup>-1</sup>, H<sub>2</sub>/CO = 2/1. These detailed results are summarized in Fig. 5 and Figs. S20-S21. As shown in Fig. 5a, compared with the monometallic CuSNTs and CoSNTs catalysts, the bimetallic CuCoSNTs catalyst exhibited higher CO conversion and lower selectivity of CH<sub>4</sub> and CO<sub>2</sub>. Therefore, in HAS from syngas, bimetallic CuCo-based catalyst was superior to single metal Cu-based or Co-based catalyst, owing to the synergistic effects of multi-active sites from CuCo. When the catalyst CuCoSNTs was hydrophobically functionalized, the CO conversion increased from 61.7% to 80.4%, and the selectivity of alcohols (ROH) also increased from 42.4% to 61.7%. The hydrophobic catalyst CuCoSNTs-c also showed the highest C<sub>2+</sub>OH selectivity and lowest CH<sub>4</sub> and CO<sub>2</sub> selectivity under such circumstance, further confirming the hydrophobic functionalized modification not only enhanced the CO conversion but also favored the selective formation of C<sub>2+</sub>OH. As expected, the hydrophobic CuCoSNTs-c catalyst had an outstanding ROH yield of 49.6%. The hierarchical hollow tubular CuCoSNTs-c

catalyst with excellent hydrophobicity hindered the water-gas shift (WGS) reaction, which enhanced the carbon-carbon coupling reaction and inhibited the formation of CH<sub>4</sub> (8.6%) and CO<sub>2</sub> (1.2%). The chain growth probability ( $\alpha$ ) value evaluated by the Anderson-Schulz-Flory (ASF) model was increased from 0.31 for the hydrophilic catalyst CuCoSNTs to 0.34 for the hydrophobic catalyst CuCoSNTs-c (Fig. 5e), and the selectivity for undesired C<sub>1</sub> by-product was suppressed to 9.8% (Fig. 5a). Moreover, the hydrophobic CuCoSNTs-c catalyst exhibited a superior C<sub>2+</sub>OH selectivity of 66.6% (including 42.3% of ethanol) than that of the hydrophilic catalyst CuCoSNTs (C<sub>2+</sub>OH selectivity of 54.8%) (Fig. 5b). The CO conversion and selectivity of products over the CuCo-based catalyst could also be adjusted by changing the ratio of Cu to Co. It is worth noting that the selectivity toward both ROH and C<sub>2+</sub>OH presented a volcano-type trend with the increasing Cu/Co ratio (Fig. S20), and hydrophobic catalyst CuCoSNTs-c (Cu<sub>5</sub>Co<sub>5</sub>SNTs-c) showed the TOF (892 h<sup>-1</sup>) for C<sub>2+</sub>OH and the space-time yield (STY) toward C<sub>2+</sub>OH (0.970 g/g<sub>cat</sub>·h) (Fig. S21). The catalyst CuCoSNTs-c mentioned in this work is Cu<sub>5</sub>Co<sub>5</sub>SNTs-c unless otherwise specified. These results confirmed that the hydrophobic functionalization promoted the intrinsic activity of CuCo-based catalysts for syngas conversion. We further compared the performance of CuCoSNTs-c with various catalysts tested previously in syngas conversion to higher alcohols. For CuCoSNTs-c catalyst, the CO<sub>2</sub> selectivity was suppressed to a low level (<2%) and the highest CO conversion was maintained concurrently. These exciting results demonstrated the excellent inhibition ability of the CuCoSNTs-c for undesired WGS reaction during the HAS process (Fig. 5d).

In addition to the catalytic activity, the durability of catalyst plays a significant role in advanced industrial applications. We evaluated the hydrophilic CuCoSNTs and hydrophobic CuCoSNTs-c catalysts in HAS from syngas under the optimum reaction conditions of 270 °C, 3 MPa, H<sub>2</sub>/CO = 2/1, and GHSV = 8000 h<sup>-1</sup> for over 360 h (the samples were collected and analyzed every 12 h). In addition to enhancing C<sub>2+</sub>OH selectivity and intrinsic activity, the hydrophobic modification markedly improved the catalyst durability. It was found that the hydrophilic catalyst CuCoSNTs underwent deactivation during the long-term reaction, not only the CO conversion declined to less than 40% after 200 h, but also the ROH selectivity significantly decreased, and the CH<sub>4</sub> selectivity continuously increased with time on stream (Fig. S22). The hydrophobic catalyst CuCoSNTs-c became remarkably stable in HAS from syngas. No significant changes in CO conversion (~80%) and alcohols selectivity (~61%) were observed over 360 h of reaction, and the undesired C<sub>1</sub> by-products (CH<sub>4</sub> and CO<sub>2</sub>) selectivity remained at < 10% with time on stream (Fig. 5c), indicating that the CuCoSNTs-c exhibited outstanding stability. In the initial stage, the CO conversion and HAs selectivity increased and maintained stable, while the methanol selectivity first decreased and then remained imperceptible changes (Fig. S23). All the results suggested that the catalyst CuCoSNTs-c was a highly efficient catalyst for converting syngas to HAs with high CO conversion, excellent alcohol selectivity, and long-time stability.

### 3.3. Electronic structure analysis and catalytic mechanism

To elucidate the mechanism of higher alcohol synthesis with the dual metal CuCo catalyst, and the peculiarities of electronic structure in this system, density functional theory (DFT) simulations have been performed employing PBE density functional [39]. The fragment of the SNTs with the incorporated CuCo catalyst was modelled by a (001) surface slab of an  $\alpha$ -quartz SiO<sub>2</sub>. It is well known that silica surfaces are often hydroxylated and from the theoretical analysis it is evident that the presence of superficial OH groups is a factor, among other, enabling the electroneutrality of the system. This fact is reflected in the model system, in which both sides of the slab are hydroxylated. Such a feature is important for the hydrogenation reactions, such as those considered in this work, since the protons of the OH-groups can be easily exchanged between the SiO<sub>2</sub>-support and the reactive species. Interestingly, OH

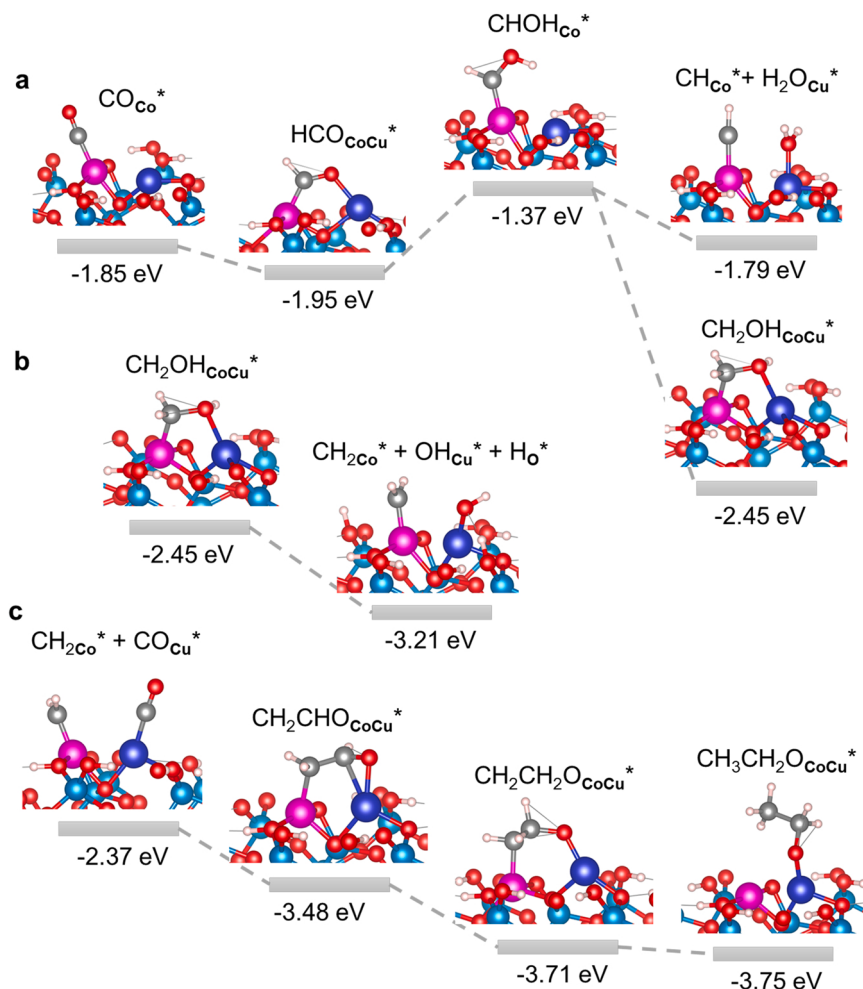


**Fig. 6.** Key steps of the HAS reaction formation on the CuCoSNTs-c catalyst. (a) CO reduction. (b) C-O bond breaking. (c) C-C coupling, followed by hydrogenation. The given energies correspond to formation reaction of the adsorbed species, computed with respect to gas phase CO, H<sub>2</sub> and pristine catalyst surface. The Co, Cu, Si, O and H atoms are denoted in magenta, deep blue, cyan, red and rose, respectively.

groups on the SiO<sub>2</sub> surface form hydrogen bonds with the neighboring oxygens aligning horizontally, instead of a typical vertical orientation of hydroxyl groups. Importantly, (001) SiO<sub>2</sub> surface had a configuration of surface oxygen atoms favorable for incorporation of CuCo catalyst (Fig. S24). Indeed, in the DFT simulation we observed that upon relaxation of CuCoSNTs-c surface the Cu<sup>2+</sup> and Co<sup>2+</sup> cations became strongly bound to the oxygen atoms, forming two and three metal-oxygen bonds, respectively, that was favorable for the catalyst stability and reproducibility. The primary step of the HAS from the CO was its adsorption on the catalytic sites. Our DFT calculations revealed that it preferably occurred on Co site, similar to previous findings on Co/Cu-N-C systems [22]. However, in contrast to Co/Cu-N-C, where CO only adsorbed on Co site, in the case of the CuCoSNTs-c, it could also adsorb on Cu and in-between Co and Cu sites, even though these adsorption modes were less favorable (Table S5).

The CO adsorption was followed by several hydrogenation steps resulting in the generation of intermediate species whose formation on the metal sites is less energetically favorable. This included HCO<sub>Co</sub>, HCOH<sub>Co</sub> and CH<sub>Co</sub>+H<sub>2</sub>O<sub>Cu</sub> moieties. Interestingly, the formation of hydrogenated species CH<sub>2</sub>OH<sub>CoCu</sub> on the catalytic site, in which C atom adsorbed on the Co site and O atom on the Cu site were more energetically favorable than the dissociative formation of CH<sub>Co</sub> and H<sub>2</sub>O<sub>Cu</sub> indicating that the successive hydrogenation of adsorbed CO moiety favorably occurred prior to C-O bond dissociation. The adsorbed CH<sub>2</sub>Co<sup>\*</sup> and OH<sub>Cu</sub><sup>\*</sup> spontaneously form back CH<sub>2</sub>OH<sub>CoCu</sub> restoring the broken C-O bond (Video S1 CH<sub>2</sub>Co-OH<sub>Cu</sub>). As for the C-O bond splitting

via formation of CH<sub>2</sub>Co<sup>\*</sup> and H<sub>2</sub>O species, it was energetically even more favorable than the formation of CH<sub>2</sub>OH<sub>CoCu</sub><sup>\*</sup>, however, the water molecule in this case spontaneously splitted via heterogeneous dissociation mechanism to OH<sub>Cu</sub><sup>\*</sup> and H<sub>2</sub>O<sup>\*</sup> (Video S2 CH<sub>2</sub>Co-H<sub>2</sub>O<sub>Cu</sub>). The same phenomenon was observed when an isolated water molecule was placed on the copper site. Thus, the water molecules, formed in the course of CO hydrogenation and C-O splitting reactions, could be dissociative re-adsorbed on the catalytic sites, forming OH species. But, as shown in Fig. 6, CH<sub>2</sub>Co<sup>\*</sup> and OH<sub>Cu</sub><sup>\*</sup> could easily recombine to form a C-O bond, reverting the direction of the entire HAS process. Therefore, it is important to promptly evacuate water molecules from the SNTs surface straight after their formation. The hydrophobic coating was determined to be essential for this purpose. As evidenced by the molecular dynamic simulations of water molecules at the silanized SiO<sub>2</sub> surface, the first ones were effectively repelled from it, methyl groups preventing their strong binding or dissociative adsorption (Video S3 Si-CH<sub>3</sub>-H<sub>2</sub>O). This favors the reaction of the C-O bond splitting both thermodynamically by eliminating water from the reaction site thus shifting the equilibrium and kinetically by preventing the formation of OH groups at the catalytic sites required to revert this reaction. Importantly, avoiding the heterolytic splitting of water at the catalytic site were also important for hindering the water gas shift reaction, since it supplied the O-containing species for CO oxidation. The impact of hydroxyls on the reversibility of C-O bond formation and the hydrophobic effect of methyl groups were in line with the increased conversion degree of CO and enhanced selectivity towards the C-C chain growth. Indeed, the CH<sub>2</sub>Co<sup>\*</sup> species

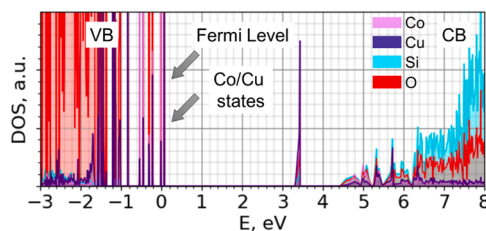


**Fig. 7.** Electronic structure of the CoCu catalyst: projected density of states. The energy of the Fermi level is set to 0 eV. In its vicinity a large density of Co and Cu metal states is concentrated, as depicted by the gray arrow.

became more accessible to the interaction with other C-containing moieties. At the next step, CO molecule was stably adsorbed on the Cu sites, which were liberated from  $\text{H}_2\text{O}$  molecules or OH groups due to the hydrophobic coating. But here in contrast to previously reported Co/Cu-N-C catalyst, there was no spontaneous C-C coupling upon a direct interaction. Instead, when  $\text{CO}_{\text{Cu}}^*$  is mono-hydrogenated and converted into  $\text{CHO}_{\text{Cu}}^*$ , the last one directly migrated towards the Co-site with the adsorbed  $\text{CH}_{2\text{Co}}^*$  enabling a C-C coupling without a barrier (Video S4  $\text{CH}_{2\text{Co}}\text{-CHO}_{\text{Cu}}$ ). The formation of the adsorbed  $\text{CH}_2\text{CHO}_{\text{CoCu}}^*$  was extremely favorable, since it involved both the C-Co, C-Cu and O-Cu interactions. This was followed by energetically favorable consecutive hydrogenation of this intermediate, leading to  $\text{CH}_2\text{CH}_2\text{O}_{\text{CoCu}}^*$  and  $\text{CH}_3\text{CH}_2\text{O}_{\text{CoCu}}^*$ . The desorption accompanied by the protonation of the last one results in the formation of ethanol.

Supplementary material related to this article can be found online at doi:10.1016/j.apcatb.2023.122840.

The observed pathway contrasts with the one for the previously reported Co/Cu-N-C system [22], that is indicative of role of the support and hydrophobic modification in the re-routing of the intermediate reaction steps.

The activity of the CuCoSNTs-c catalyst is due not only to the synergistic effect of CuCo sites in the adsorption of intermediate species, but also due to its unique electronic structure. The coupling of Cu and Co at the reactive sites generated a large density of states near the Fermi level (Fig. 7). Upon the homolytic hydrogen adsorption on the oxygen atoms of the silica support, the resulting reduction electrons easily occupy [43, 73] the empty states localized on Cu or Co. In return, during the reduction of CO and further reaction intermediates, both the electrons and the adsorbed protons can transfer to the C-containing adsorbates to reduce them. All these mentioned features underline the high CO conversion ratio and selectivity toward HAs of the presented CuCoSNTs-c

catalyst.

The formation path of ethanol and the inhibition mechanism of  $\text{CO}_2$  were illustrated in Fig. 8. During the HAS reaction, the adsorbed  $\text{CO}^*$  and  $\text{H}^*$  on the surface of CuCo species were reacted to form  $\text{CH}_x^*$  species, and C-C coupling and hydrogenation reactions would further produce various alcohols and hydrocarbons. The chemisorbed  $\text{O}^*$  formed by CO dissociation could react with the chemisorbed  $\text{H}^*$  from dissociated  $\text{H}_2$  to form  $\text{H}_2\text{O}$ . Re-adsorption of  $\text{H}_2\text{O}$  on the surface CuCo species of hydrophilic CuCoSNTs and reaction with  $\text{CO}^*$  would form  $\text{CO}_2$  through the WGS reaction (Fig. 8a). The inhibited  $\text{H}_2\text{O}$  adsorption and departure timely from the hydrophobic CuCoSNTs-c further suppressed the WGS reaction, so the  $\text{CO}_2$  selectivity over the hydrophobic CuCoSNTs-c catalyst during HAS was reduced (Fig. 8b). Inhibition of the WGS reaction on hydrophobic CuCoSNTs-c would increase the amount of  $\text{CO}^*$ , which would react with the  $\text{CH}_x$  to form ethanol. As a result, the ethanol selectivity increased from 33.2% of CuCoSNTs to 42.3% of CuCoSNTs-c.

#### 4. Conclusion

To summarize, a hydrophobic tubular CuCoSNTs-c catalyst with hierarchical porous structure was reported and employed for HAS from syngas. The as-prepared CuCoSNTs-c exhibited exceptional catalytic performance with a CO conversion of 80.4%, ROH selectivity of 49.6%, STY toward  $\text{C}_2\text{+OH}$  of 0.970 g/g<sub>cat</sub>·h, and outstanding stability over 360 h of reaction, which places this hydrophobic catalyst as one of the best performing catalysts for HAS. In the catalyst design, CuCoSNTs-c with mouth-open end morphology and mesoporous wall with sufficiently exposed active sites of CuCo will favor the diffusion and adsorption-desorption of syngas. The hydrophobic property of the CuCoSNTs-c catalyst increases the selectivity of HAs and effectively inhibits the formation of  $\text{C}_1$  by-products of  $\text{CH}_4$  and  $\text{CO}_2$ . DFT calculation further confirms that the reaction of the C-O bond splitting is favored both thermodynamically by eliminating water from the reaction sites, thus shifting the equilibrium and kinetically by preventing the formation of OH groups at the catalytic sites required to revert this reaction. We anticipate this hydrophobic tubular catalyst reported in this work will inspire the catalyst design in the field of catalysis especially in the water-involving catalytic applications.

#### CRediT authorship contribution statement

G.C. conducted the study. O.S. and M.S. determined the electronic structure analysis and catalytic mechanism. S.Y. and L.P. supervised the

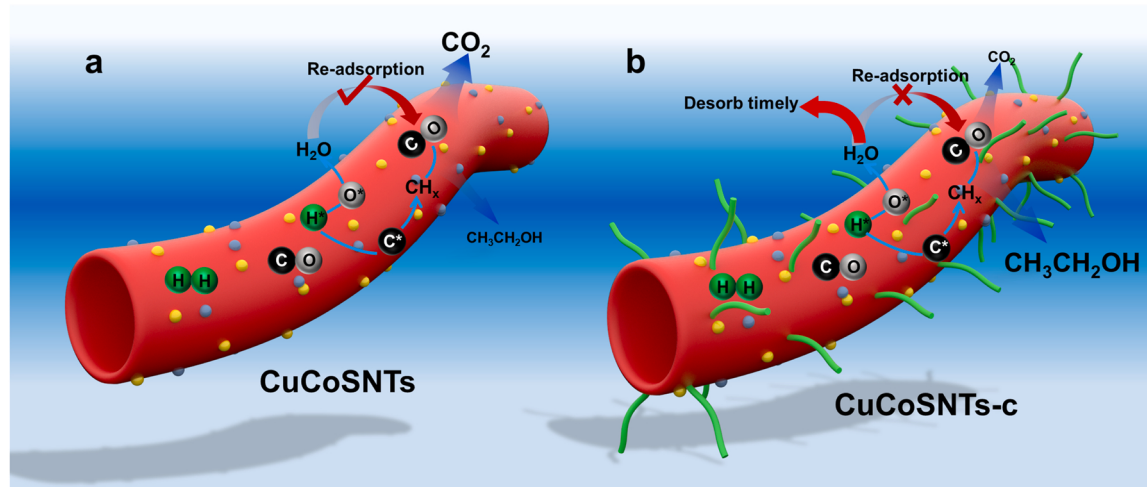


**Fig. 8.** Proposed reaction mechanism with (a) hydrophilic CuCoSNTs and (b) hydrophobic CuCoSNTs-c as catalysts, respectively. Hydrophobic modification inhibits  $\text{CO}_2$  formation effectively during the HAS process.

work. **G.Y., T.X., Q.L** implemented some experiments. **D.S** analyzed the EXAFS and XANES data. **M. L** analyzed the XPS data. **I.A., Z.W., T.L., X. Z., and L.L** discussed the results. **G.C., S.Y. and L.P** wrote the manuscript. All the authors approved the manuscript.

## Declaration of Competing Interest

The authors declare that they have no known competing financial interests or personal relationships that could have appeared to influence the work reported in this paper.

## Data availability

Data will be made available on request.

## Acknowledgements

The authors gratefully acknowledge the National Key Research and Development Program of China (2019YFB1503903). **S.Y.** sincerely acknowledges the financial support from the Nanqiang Young Top-notch Talent Fellowship from Xiamen University. The research is carried out using the equipment of the shared research facilities of HPC computing resources at Lomonosov Moscow State University. The Siberian Branch of the Russian Academy of Sciences (SB RAS) Siberian Supercomputer Center is gratefully acknowledged for providing supercomputer facilities.

## Appendix A. Supporting information

Supplementary data associated with this article can be found in the online version at [doi:10.1016/j.apcatb.2023.122840](https://doi.org/10.1016/j.apcatb.2023.122840).

## References

- [1] M. Ao, G.H. Pham, J. Sunarso, M.O. Tade, S. Liu, Active centers of catalysts for higher alcohol synthesis from syngas: a review, *ACS Catal.* 8 (2018) 7025–7050.
- [2] H.T. Luk, C. Mondelli, D.C. Ferré, J.A. Stewart, J. Pérez-Ramírez, Status and prospects in higher alcohols synthesis from syngas, *Chem. Soc. Rev.* 46 (2017) 1358–1426.
- [3] J. Kang, S. He, W. Zhou, Z. Shen, Y. Li, M. Chen, Q. Zhang, Y. Wang, Single-pass transformation of syngas into ethanol with high selectivity by triple tandem catalysis, *Nat. Commun.* 11 (2020) 827.
- [4] X. Luan, Z. Ren, X. Dai, X. Zhang, J. Yong, Y. Yang, H. Zhao, M. Cui, F. Nie, X. Huang, Selective conversion of syngas into higher alcohols via a reaction-coupling strategy on multifunctional relay catalysts, *ACS Catal.* 10 (2020) 2419–2430.
- [5] F. Zeng, X. Xi, H. Cao, Y. Pei, H.J. Heeres, R. Palkovits, Synthesis of mixed alcohols with enhanced  $C_{3+}$  alcohol production by CO hydrogenation over potassium promoted molybdenum sulfide, *Appl. Catal. B Environ.* 246 (2019) 232–241.
- [6] N. Yang, J.S. Yoo, J. Schumann, P. Bothra, J.A. Singh, E. Valle, F. Aibild-Pedersen, J.K. Norskov, S.F. Bent, Rh-MnO interface sites formed by atomic layer deposition promote syngas conversion to higher oxygenates, *ACS Catal.* 7 (2017) 5746–5757.
- [7] T. Qin, T. Lin, X. Qi, C. Wang, L. Li, Z. Tang, L. Zhong, Y. Sun, Tuning chemical environment and synergistic relay reaction to promote higher alcohols synthesis via syngas conversion, *Appl. Catal. B Environ.* 285 (2021), 119840.
- [8] Y. Li, W. Gao, M. Peng, J. Zhang, J. Sun, Y. Xu, S. Hong, X. Liu, X. Liu, M. Wei, B. Zhang, D. Ma, Interfacial  $Fe_5C_2$ -Cu catalysts toward low-pressure syngas conversion to long-chain alcohols, *Nat. Commun.* 11 (2020) 61.
- [9] Y. Xu, X. Li, J. Gao, J. Wang, G. Ma, X. Wen, Y. Yang, Y. Li, M. Ding, A hydrophobic  $FeMn@Si$  catalyst increases olefins from syngas by suppressing C1 by-products, *Science* 371 (2021) 610–613.
- [10] G. Chen, T. Lei, Z. Wang, S. Liu, X. He, Q. Guan, X. Xin, H. Xu, Preparation of higher alcohols by biomass-based syngas from wheat straw over  $CoCuK/ZrO_2-SiO_2$  catalyst, *Ind. Crops Prod.* 131 (2019) 54–61.
- [11] Y. Xiang, N. Kruse, Tuning the catalytic CO hydrogenation to straight- and long-chain aldehydes/alcohols and olefins/paraffins, *Nat. Commun.* 7 (2016) 13058.
- [12] T. Lin, X. Qi, X. Wang, L. Xia, C. Wang, F. Yu, H. Wang, S. Li, L. Zhong, Y. Sun, Direct production of higher oxygenates by syngas conversion over a multifunctional catalyst, *Angew. Chem. Int. Ed.* 58 (2019) 4627–4631.
- [13] H. Guo, H. Zhang, F. Peng, H. Yang, L. Xiong, C. Wang, C. Huang, X. Chen, L. Ma, Effects of Cu/Fe ratio on structure and performance of attapulgite supported  $CuFeCo$ -based catalyst for mixed alcohols synthesis from syngas, *Appl. Catal. A Gen.* 503 (2015) 51–61.
- [14] C. Huang, C. Zhu, M. Zhang, J. Chen, K. Fang, Design of efficient  $ZnO/ZrO_2$  modified  $CuCoAl$  catalysts for boosting higher alcohol synthesis in syngas conversion, *Appl. Catal. B Environ.* 300 (2022), 120739.
- [15] X. Ning, Z. An, J. He, Remarkably efficient CoGa catalyst with uniformly dispersed and trapped structure for ethanol and higher alcohol synthesis from syngas, *J. Catal.* 340 (2016) 236–247.
- [16] Z. Zeng, Z. Li, T. Guan, S. Guo, Z. Hu, J. Wang, A. Rykov, J. Lv, S. Huang, Y. Wang, X. Ma, CoFe alloy carbide catalysts for higher alcohols synthesis from syngas: Evolution of active sites and Na promoting effect, *J. Catal.* 405 (2022) 430–444.
- [17] Z. Li, Z. Hu, Z. Zeng, S. Guo, J. Lv, S. Huang, Y. Wang, X. Ma, Lamellar-structured silicate derived highly dispersed  $CoCu$  catalyst for higher alcohol synthesis from syngas, *Ind. Eng. Chem. Res.* 61 (2022) 6859–6871.
- [18] X. Dong, X.-L. Liang, H.-Y. Li, G.-D. Lin, P. Zhang, H.-B. Zhang, Preparation and characterization of carbon nanotube-promoted  $Co-Cu$  catalyst for higher alcohol synthesis from syngas, *Catal. Today* 147 (2009) 158–165.
- [19] Z. Li, Z. Zeng, D. Yao, S. Fan, S. Guo, J. Lv, S. Huang, Y. Wang, X. Ma, High-performance  $CoCu$  catalyst encapsulated in KIT-6 for higher alcohol synthesis from syngas, *ACS Sustain. Chem. Eng.* 8 (2020) 200–209.
- [20] L. Zhao, J. Duan, Q. Zhang, Y. Li, K. Fang, Preparation, structural characteristics, and catalytic performance of  $Cu-Co$  alloy supported on Mn-Al oxide for higher alcohol synthesis via syngas, *Ind. Eng. Chem. Res.* 57 (2018) 14957–14966.
- [21] Y. Xiang, R. Barbosa, N. Kruse, Higher alcohols through CO hydrogenation over  $CoCu$  catalysts: influence of precursor activation, *ACS Catal.* 4 (2014) 2792–2800.
- [22] G. Chen, O.A. Syzantseva, M.A. Syzantseva, S. Yang, G. Yan, L. Peng, C. Cao, W. Chen, Z. Wang, F. Qin, T. Lei, X. Zeng, L. Lin, W. Song, B. Han, Construction of synergistic Co and Cu diatomic sites for enhanced higher alcohol synthesis, *CCS Chem.* 5 (2023) 851–864.
- [23] G. Chen, Y. Feng, Z. Wang, G. Yan, Z. Si, Y. Sun, X. Tang, S. Yang, T. Lei, X. Zeng, L. Lin, *In situ* encapsulated  $CoCo@M-SiO_2$  for higher alcohol synthesis from biomass-derived syngas, *ACS Sustain. Chem. Eng.* 9 (2021) 5910–5923.
- [24] N. Tien-Thao, M.H. Zahedi-Niaki, H. Alamdar, S. Kaliaguine, Conversion of syngas to higher alcohols over nanosized  $LaCo_{0.7}Cu_{0.3}O_3$  perovskite precursors, *Appl. Catal. A Gen.* 326 (2007) 152–163.
- [25] Y. Xiang, V. Chitrav, P. Liddicoat, P. Felfer, J. Cairney, S. Ringer, N. Kruse, Long-chain terminal alcohols through catalytic CO hydrogenation, *J. Am. Chem. Soc.* 135 (2013) 7111–7117.
- [26] A. Cao, G. Liu, L. Wang, J. Liu, Y. Yue, L. Zhang, Y. Liu, Growing layered double hydroxides on CNTs and their catalytic performance for higher alcohol synthesis from syngas, *J. Mater. Sci.* 51 (2016) 5216–5231.
- [27] K. Sun, Z. Liu, S. Song, W. Liu, P. Wang, T. Zhang, Y. Xue, Y. Wang, Y. Tan, Effect of hydroxyl groups on  $CoCuMg$  nanosheets for ethanol and higher alcohol synthesis from syngas, *Ind. Eng. Chem. Res.* 60 (2021) 2388–2399.
- [28] K. Sun, M. Tan, Y. Bai, X. Gao, P. Wang, N. Gong, T. Zhang, G. Yang, Y. Tan, Design and synthesis of spherical-plateletlike ternary copper-cobalt-manganese catalysts for direct conversion of syngas to ethanol and higher alcohols, *J. Catal.* 378 (2019) 1–16.
- [29] G. Prieto, S. Beijer, M.L. Smith, M. He, Y. Au, Z. Wang, D.A. Bruce, K.P. deJong, J. J. Spivey, P.E. deJongh, Design and synthesis of copper-cobalt catalysts for the selective conversion of synthesis gas to ethanol and higher alcohols, *Angew. Chem. Int. Ed.* 126 (2014) 6515–6519.
- [30] W.-G. Cui, Y.-T. Li, H. Zhang, Z.-C. Wei, B.-H. Gao, J.-J. Dai, T.-L. Hu, *In situ* encapsulated  $Co/MnO$  nanoparticles inside quasi-MOF-74 for the higher alcohols synthesis from syngas, *Appl. Catal. B Environ.* 278 (2020), 119262.
- [31] Z. Li, G. Luo, T. Chen, Z. Zeng, S. Guo, J. Lv, S. Huang, Y. Wang, X. Ma, Bimetallic  $CoCu$  catalyst derived from *in-situ* grown Cu-ZIF-67 encapsulated inside KIT-6 for higher alcohol synthesis from syngas, *Fuel* 278 (2020), 118292.
- [32] W. Gao, Y. Zhao, H. Chen, H. Chen, Y. Li, S. He, Y. Zhang, M. Wei, D.G. Evans, X. Duan, Core-shell  $Co@Cu(CuCo-alloy)/Al_2O_3$  catalysts for the synthesis of higher alcohols from syngas, *Green Chem.* 17 (2015) 1525–1534.
- [33] W. Fang, C. Wang, Z. Liu, L. Wang, L. Liu, H. Li, S. Xu, A. Zheng, X. Qin, L. Liu, F.-S. Xiao, Physical mixing of a catalyst and a hydrophobic polymer promotes CO hydrogenation through dehydration, *Science* 377 (2022) 406–410.
- [34] J. Wang, G. Zhang, J. Zhu, X. Zhang, F. Ding, A. Zhang, X. Guo, C. Song,  $CO_2$  hydrogenation to methanol over  $In_2O_3$ -based catalysts: from mechanism to catalyst development, *ACS Catal.* 11 (2021) 1406–1423.
- [35] J. Wang, G. Li, Z. Li, C. Tang, Z. Feng, H. An, H. Liu, T. Liu, C. Li, A highly selective and stable  $ZnO-ZrO_2$  solid solution catalyst for  $CO_2$  hydrogenation to methanol, *Sci. Adv.* 3 (2017), e1701290.
- [36] J. Qu, W. Li, C.-Y. Cao, X.-J. Yin, L. Zhao, J. Bai, Z. Qin, W.-G. Song, Metal silicate nanotubes with nanostructured walls as superb adsorbents for uranyl ions and lead ions in water, *J. Mater. Chem.* 22 (2012) 17222–17226.
- [37] B. Xu, Y. Cui, W. Wang, S. Li, C. Lyu, S. Wang, W. Bao, H. Wang, M. Qin, Z. Liu, W. Wei, H. Liu, Immunomodulation-enhanced nanzyme-based tumor catalytic therapy, *Adv. Mater.* 32 (2020).
- [38] S.-M. Hao, J. Qu, Z.-S. Zhu, X.-Y. Zhang, Q.-Q. Wang, Z.-Z. Yu, Hollow manganese silicate nanotubes with tunable secondary nanostructures as excellent Fenton-type catalysts for dye decomposition at ambient temperature, *Adv. Funct. Mater.* 26 (2016) 7334–7342.
- [39] J.P. Perdew, K. Burke, M. Ernzerhof, Generalized gradient approximation made simple, *Phys. Rev. Lett.* 77 (1996) 3865–3868.
- [40] P. Giannozzi, O. Andreussi, T. Brumme, O. Bunau, M. Buongiorno Nardelli, M. Calandra, R. Car, C. Cavazzoni, D. Ceresoli, M. Cococcioni, N. Colonna, I. Carnimeo, A. Dal Corso, S. de Gironcoli, P. Delugas, R.A. DiStasio, A. Ferretti, A. Floris, G. Fratesi, G. Fugallo, R. Gebauer, U. Gerstmann, F. Giustino, T. Gorni, J. Jia, M. Kawamura, H.-Y. Ko, A. Kokalj, E. Küçükbenli, M. Lazzari, M. Marsili, N. Marzari, F. Mauri, N.L. Nguyen, H.-V. Nguyen, A. Otero-de-la-Roza, L. Paulatto, S. Poncé, D. Rocca, R. Sabatini, B. Santra, M. Schlipf, A.P. Seitsonen, A. Smogunov, I. Timrov, T. Thonhauser, P. Umari, N. Vast, X. Wu, S. Baroni, Advanced

capabilities for materials modelling with Quantum ESPRESSO, *J. Phys. Condens. Matter* 29 (2017), 465901.

[41] A. Dal, Corso, Pseudopotentials periodic table: from H to Pu, *Comput. Mater. Sci.* 95 (2014) 337–350.

[42] A. Rappe, K. Rabe, E. Kaxiras, J. Joannopoulos, Erratum: optimized pseudopotentials [*Phys. Rev. B* 41, 1227 (1990)], *Phys. Rev. B* 41 (1990) 1227–1230.

[43] Z. Helali, A. Jedidi, O.A. Syzgantseva, M. Calatayud, C. Minot, Scaling reducibility of metal oxides, *Theor. Chem. Acc.* 136 (2017) 100.

[44] S. Grimme, C. Bannwarth, P. Shushkov, A robust and accurate tight-binding quantum chemical method for structures, vibrational frequencies, and noncovalent interactions of large molecular systems parametrized for all spd-block elements (Z = 1–86), *J. Chem. Theory Comput.* 13 (2017) 1989–2009.

[45] S. Grimme, J. Antony, S. Ehrlich, H. Krieg, A consistent and accurate ab initio parametrization of density functional dispersion correction (DFT-D) for the 94 elements H–Pu, *J. Chem. Phys.* 132 (2010), 154104.

[46] T.D. Kühne, M. Iannuzzi, M. Del Ben, V.V. Rybkin, P. Seewald, F. Stein, T. Laino, R. Z. Khalilullin, O. Schütt, F. Schiffmann, D. Golze, J. Wilhelm, S. Chulkov, M. H. Bani-Hashemian, V. Weber, U. Borstnik, M. Taillefumier, A.S. Jakobovits, A. Lazzaro, H. Pabst, T. Müller, R. Schade, M. Guidon, S. Andermatt, N. Holmberg, G.K. Schenter, A. Hehn, A. Bussy, F. Belleflamme, G. Tabacchi, A. Glööb, M. Lass, I. Bethune, C.J. Mundy, C. Plessl, M. Watkins, J. VandeVondele, M. Krack, J. Hutter, CP2K: An electronic structure and molecular dynamics software package—Quickstep: Efficient and accurate electronic structure calculations, *J. Chem. Phys.* 152 (2020), 194103.

[47] K. Momma, F. Izumi, VESTA 3 for three-dimensional visualization of crystal, volumetric and morphology data, *J. Appl. Crystallogr.* 44 (2011) 1272–1276.

[48] W. Humphrey, A. Dalke, K. Schulten, VMD: visual molecular dynamics, *J. Mol. Graph.* 14 (1996) 33–38.

[49] S.-W. Bian, Z. Ma, L.-S. Zhang, F. Niu, W.-G. Song, Silica nanotubes with mesoporous walls and various internal morphologies using hard/soft dual templates, *Chem. Commun.* (2009) 1261–1263.

[50] C. Ciotea, B. Dragoi, A. Ungureanu, A. Chiriac, S. Petit, S. Royer, E. Dumitriu, Nanosized transition metals in controlled environments of phyllosilicate–mesoporous silica composites as highly thermostable and active catalysts, *Chem. Commun.* 49 (2013) 7665–7667.

[51] M.V. Sivaiah, S. Petit, J. Barrault, C. Batiot-Dupeyrat, S. Valange, CO<sub>2</sub> reforming of CH<sub>4</sub> over Ni-containing phyllosilicates as catalyst precursors, *Catal. Today* 157 (2010) 397–403.

[52] M.V. Sivaiah, S. Petit, M.F. Beaufort, D. Eyidi, J. Barrault, C. Batiot-Dupeyrat, S. Valange, Nickel based catalysts derived from hydrothermally synthesized 1:1 and 2:1 phyllosilicates as precursors for carbon dioxide reforming of methane, *Microporous Mesoporous Mater.* 140 (2011) 69–80.

[53] G.J. de, A.A. Soler-Illia, E.L. Crepaldi, D. Grosso, C. Sanchez, Block copolymer-templated mesoporous oxides, *Curr. Opin. Colloid Interface Sci.* 8 (2003) 109–126.

[54] X. Tan, K. Sun, Z. Zhuang, B. Hu, Y. Zhang, Q. Liu, C. He, Z. Xu, C. Chen, H. Xiao, C. Chen, Stabilizing copper by a reconstruction-resistant atomic Cu–O–Si interface for electrochemical CO<sub>2</sub> reduction, *J. Am. Chem. Soc.* 145 (2023) 8656–8664.

[55] L. Shi, D. Li, B. Hou, Y. Sun, Organic modification of SiO<sub>2</sub> and its influence on the properties of Co-based catalysts for Fischer-Tropsch synthesis, *Chin. J. Catal.* 28 (2007) 999–1002.

[56] W. Hu, L. Liu, Y. Fan, M. Huang, Facile synthesis of mesoporous copper silicate aggregates for highly selective enrichment of hemoglobin, *Microchem. J.* 167 (2021), 106256.

[57] S. Bawaked, K. Narasimharao, Structural and catalytic properties of copper silicate nanomaterials, *Sci. Rep.* 10 (2020) 518.

[58] Y. Li, K. Nie, Q. Tang, G. Tian, J. Liang, In-situ synthesis of duster-like hollow mesoporous copper silicate composites for high-efficiency adsorption of aflatoxin B<sub>1</sub> from water, *Microporous Mesoporous Mater.* 346 (2022), 112317.

[59] Y. Liu, Y. Wei, M. Liu, Y. Bai, X. Wang, S. Shang, C. Du, W. Gao, J. Chen, Y. Liu, Face-to-face growth of wafer-scale 2D semiconducting MOF films on dielectric substrates, *Adv. Mater.* 33 (2021), 2007741.

[60] J. Park, A.C. Hinckley, Z. Huang, D. Feng, A.A. Yakovenko, M. Lee, S. Chen, X. Zou, Z. Bao, Synthetic routes for a 2D semiconductive copper hexahydroxybenzene metal-organic framework, *J. Am. Chem. Soc.* 140 (2018) 14533–14537.

[61] M.S. AlSalhi, S. Devanesan, N.N. Asemi, M. Aldawsari, Construction of SnO<sub>2</sub>/CuO/rGO nanocomposites for photocatalytic degradation of organic pollutants and antibacterial applications, *Environ. Res.* 222 (2023), 115370.

[62] T. Xue, J.-M. Lee, Capacitive behavior of mesoporous Co(OH)<sub>2</sub> nanowires, *J. Power Sources* 245 (2014) 194–202.

[63] L. Li, H. Qian, J. Ren, CdTe@Co(OH)<sub>2</sub> (core-shell) nanoparticles: aqueous synthesis and characterization, *Chem. Commun.* (2005) 4083–4085.

[64] Y. Xu, Z. Liu, D. Chen, Y. Song, R. Wang, Synthesis and electrochemical properties of porous  $\alpha$ -Co(OH)<sub>2</sub> and Co<sub>3</sub>O<sub>4</sub> microspheres, *Prog. Nat. Sci. Mater.* 27 (2017) 197–202.

[65] L. Kong, S. Dang, B. Yao, Y. Li, B. Chen, X. Hua, G. Tian, Preparation of pleated flower-like manganese-cobalt-silicate bimetallic electrode materials for supercapacitors, *J. Colloid Interface Sci.* 628 (2022) 670–681.

[66] J. Ji, Y. Zhao, Y. Zhang, X. Dong, C. Meng, X. Liu, Fabrication of phosphorus-doped cobalt silicate with improved electrochemical properties, *Molecules* 26 (2021) 6240.

[67] Y. Cheng, Y. Zhang, H. Jiang, X. Dong, C. Meng, Z. Kou, Coupled cobalt silicate nanobelts-on-nanobelt hierarchy structure with reduced graphene oxide for enhanced supercapacitive performance, *J. Power Sources* 448 (2020), 227407.

[68] Y. Zhang, C. Wang, H. Jiang, Q. Wang, J. Zheng, C. Meng, Cobalt-nickel silicate hydroxide on amorphous carbon derived from bamboo leaves for hybrid supercapacitors, *Chem. Eng. J.* 375 (2019), 121938.

[69] Y. Shao, M. Kosari, S. Xi, H.C. Zeng, Single solid precursor-derived three-dimensional nanowire networks of CuZn-silicate for CO<sub>2</sub> hydrogenation to methanol, *ACS Catal.* (2022) 5750–5765.

[70] X. Dong, Y. Yu, X. Jing, H. Jiang, T. Hu, C. Meng, C. Huang, Y. Zhang, Sandwich-like honeycomb Co<sub>2</sub>SiO<sub>4</sub>/rGO/honeycomb Co<sub>2</sub>SiO<sub>4</sub> structures with enhanced electrochemical properties for high-performance hybrid supercapacitor, *J. Power Sources* 492 (2021), 229643.

[71] T. Hu, Y. Wang, X. Dong, Y. Mu, X. Pei, X. Jing, M. Cui, C. Meng, Y. Zhang, Cobalt silicate: critical synthetic conditions affect its electrochemical properties for energy storage and conversion, *Dalton Trans.* 51 (2022) 2815–2826.

[72] M.C. Biesinger, Accessing the robustness of adventitious carbon for charge referencing (correction) purposes in XPS analysis: insights from a multi-user facility data review, *Appl. Surf. Sci.* 597 (2022), 153681.

[73] M.A. Syzgantseva, C.P. Ireland, F.M. Ebrahim, B. Smit, O.A. Syzgantseva, Metal substitution as the method of modifying electronic structure of metal-organic frameworks, *J. Am. Chem. Soc.* 141 (2019) 6271–6278.